Supplementary Information

Manipulating diffusion energy barrier in Graphene Oxide subnanochannels for precise radionuclide separation and CsCl recovery

Ziwen Dai[1], Pengrui Jin[2, 3*], Jing Wang[1], Hao Tan[1], Genyuan Zhang[1], Huying Li[1], Dandan Su[1,4], Sha Liang[1], Jiakuan Yang[1], Mihail Barboiu[4], Bart Van der Bruggen[2,5], Shushan Yuan[1*]

1 Hubei Key Laboratory of Multi-media Pollution Cooperative Control in Yangtze Basin, School of Environmental Science & Engineering, Huazhong University of Science and Technology, Wuhan, Hubei, 430074, China

2 Department of Chemical Engineering, KU Leuven, Celestijnenlaan 200F, 3001 Heverlee, Belgium

3 Department of Chemical Engineering, University of Bath, Claverton Down, Bath, BA2 7AY, U.K.

4 Institut Européen des Membranes, Université of Montpellier, Pl. Eugène Bataillon, CC047, 34095, Montpellier, France

5 Department of Chemical and Biochemical Engineering, Korea University, 145 Anam-Ro, Sungbuk-Gu, Seoul 02841, Republic of Korea

Corresponding authors emails：pj665@bath.ac.uk; yuanss@hust.edu.cn

Table of Contents

Supplementary Figures

Supplementary Fig. 17. Binding energy between EDTA and Cs^+ (a), La^{3+} (b).

Supplementary Fig. 18. E_a of different ions for GO membrane.

Supplementary Fig. 19. Conductance of CsCl of different concentration for GO and GO-EDTA-1.5 membrane.

Supplementary Fig. 20. ΔS and ΔH of CsCl and $LaCl_3$ for GO and GO-EDTA.

Supplementary Fig. 21. Representative QCM results.

Supplementary Fig. 22. Partition energy barrier of GO (a) and GO-EDTA-1.5 (b) membranes.

Supplementary Fig. 23. Molecular dynamics simulation model.

Supplementary Fig. 24. The radial distribution function and coordination number of Cs^+ in the bulk solution and GO-EDTA channels.

Supplementary Fig. 25. The radial distribution function and coordination number of La^{3+} in the bulk solution and GO-EDTA channels.

Supplementary Fig. 26. Photos of Original, ultrasonic treatment and acid soaking treatment for GO and GO-EDTA membrane.

Supplementary Fig. 27. Ion selectivity of GO and GO-EDTA membranes in electrodialysis testing methods.

Supplementary Fig. 28. Schematic diagram of the application of commercial NF90 membrane in nuclear wastewater treatment and CsCl recovery.

Supplementary Fig. 29. Ion-selective of commercial NF90 membrane in the treatment of nuclear wastewater by electrodialysis testing methods.

Supplementary Fig. 30. SEM images of the surfaceand cross-section of the GO-EDTA membrane after irradiation treatment.

Supplementary Fig. 31. FTIR spectrum of the GO-EDTA and GO-EDTA membrane after irradiation treatment.

Supplementary Fig. 32. C1s (a) and N1s (b) spectrum of the GO-EDTA membrane after irradiation treatment.

Supplementary Fig. 33. Ion selectivity of GO and GO-EDTA membranes after γ-ray irradiation treatment (100 kGy).

Supplementary Tables

Supplementary Table 1. The physical properties of related ions in this study.

Supplementary Table 2. Comparison of the CsCl permeance and Cs^{+}/Sr^{2+} selectivity of several membranes reported in the literature.

Supplementary References.

Materials

Graphene oxide powder was purchased from Xianfeng Nanomaterials Technology Co., Ltd. EDTA-2Na (≥98%), HCl (12 mol/L), KCl, NaCl, CsCl, $CaCl_2$, $SrCl_2$, $LaCl_3 \cdot 7H_2O$ were purchased from Alladin. Polyethersulfone (PES) substrate (0.1 μm, 47 mm) was purchased from Longjin Membrane Industry Technology Co., Ltd. All the chemicals were used without further purification.

Fabrication of Membranes

The GO nanosheets dispersion (0.1 mg/mL) was obtained by dissolving 10 mg of GO powder in 100 mL deionized water and ultrasonic for 90 minutes, centrifuging at 7000 rpm for 10 minutes for three times to remove the residue. EDTA-2Na solutions with concentrations of 0, 0.5, 1.0, 1.5 and 2.0 mg/mL, respectively were prepared. The GO dispersion (0.1 mg/mL) was added to 15 mL EDTA-2Na solution, followed by continuous stirring at room temperature for 6 h. Then the GO-EDTA mixture solution was poured into a suction filtration device sandwiched with a PES membrane. After standing for 10 min, the mixture solution was filtered with a pressure of 1.0 bar for 10 min. After there was no solution on the membrane surface, filtration was continued for 10 min to remove the residual solution in the interlayer spacing. The obtained membrane was vacuum-dried at 70 °C for 24 h. By the difference in EDTA-2Na concentration, the synthesized membranes were named as GO, GO-EDTA-0.5, GO-EDTA-1.0, GO-EDTA-1.5, GO-EDTA-2.0, respectively. At the same time, membranes with different thickness were also obtained by adjusting the different loading amounts of GO (0.15, 0.3, 0.6 and 1.2 g/m^2).

Ion Conductance by Linear Sweep Voltammetry (LSV)

The ion transport behavior of various membranes was evaluated by linear sweep voltammetry (LSV) in a laboratory-scale electrodialysis cell. For each tested single-electrolyte solution, the ionic strength was varied from 10^{-9} to 0.1 mol/L. The applied electric potential was swept from −1 V to +1 V at a scan rate of 5 mV/s, and the resulting current response was recorded. The membrane assembly was placed between two compartments, each filled with the same single-electrolyte solution. Silver/silver

chloride electrodes were positioned in each compartment for all I–V measurements. The ionic conductance was determined from the slope of the LSV curve.

Characterizations

Surface and cross-sectional morphologies of the GO and GO-EDTA membranes were examined using a TESCAN MIRA LMS scanning electron microscope (SEM) at 3 kV. Nanosheet transmission electron microscopy (TEM) imaging was conducted on a JEOL JEM ARM200F. A Bruker Dimension Icon atomic force microscope (AFM) provided both topographical and Kelvin probe force microscopy (KPFM) images. Functional group changes in the membranes were analyzed by attenuated total reflection infrared (ATR-IR) spectroscopy on a Thermo Scientific Nicolet iS50R. AFM also yielded membrane roughness and thickness data, while KPFM measured surface potentials. X-ray photoelectron spectroscopy (XPS) was performed with a Thermo Kalpha instrument. Interlayer spacing was further determined by X-ray diffraction (XRD) on a Shimadzu XRD-7000 (Cu-Kα, 2θ range 5°–15°). Inductively coupled plasma optical emission spectrometry (ICP-OES) was carried out on a Leeman Labs Prodigy Plus. Membrane samples received γ-ray irradiation (^{60}Co source) at a total dose of 10 and 100 kGy with a dose rate of 5 kGy/h, using a JC-200 cobalt-source irradiator from Beijing Jinhui Irradiation Technology Application Co., Ltd.

XPS peak fitting

The XPS analysis and peak fitting were carried out using the Thermo Avantage software. All XPS spectra were fitted using a GL(30) peak shape with a Shirley background. The fitting algorithm was Powell. The FWHM of all the fitted peaks is limited to between 0.5 and 2.0 eV. The binding energy is fixed according to the literature values. The charge correction is calibrated based on the binding energy of C-C at 284.8 eV as the standard. All the samples were subjected to the same fitting procedure. The final fitted data was obtained by performing steps such as subtracting the baseline, peak finding, and charge correction on the original data.

Details of XPS peak fitting data

Membrane	Atomic orbital	Chemical bond	Peak (BE)	FWHM (eV)
GO	C1s	C-C	284.4	1.42
		C-O	286.8	1.28
		C=O	288.1	1.87
GO-EDTA-0.5	C1s	C-C	284.8	1.06
		C-N	285.3	1.92
		C-O	286.5	1.59
		C=O	288.2	1.93
	N1s	C-N	399.7	1.81
		N-H+	402.5	1.92
GO-EDTA-1.0	C1s	C-C	284.8	1.01
		C-N	285.2	1.92
		C-O	286.7	1.22
		C=O	288.4	1.92
	N1s	C-N	399.9	1.62
		N-H+	402.8	1.91
GO-EDTA-1.5	C1s	C-C	284.8	1.06
		C-N	285.1	1.90
		C-O	286.6	1.09
		C=O	288.4	1.61
	N1s	C-N	399.9	1.72
		N-H+	402.5	1.87
GO-EDTA-2.0	C1s	C-C	284.8	1.01
		C-N	285.2	1.85
		C-O	286.6	1.15
		C=O	288.1	1.86
	N1s	C-N	399.4	1.38
		N-H+	401.5	1.98
GO-EDTA-1.5 (After irradiation)	C1s	C-C	284.8	1.49
		C-N	285.4	0.95
		C-O	286.9	1.05
		C=O	288.8	1.96
	N1s	C-N	399.8	1.54
		N-H+	402.0	1.33

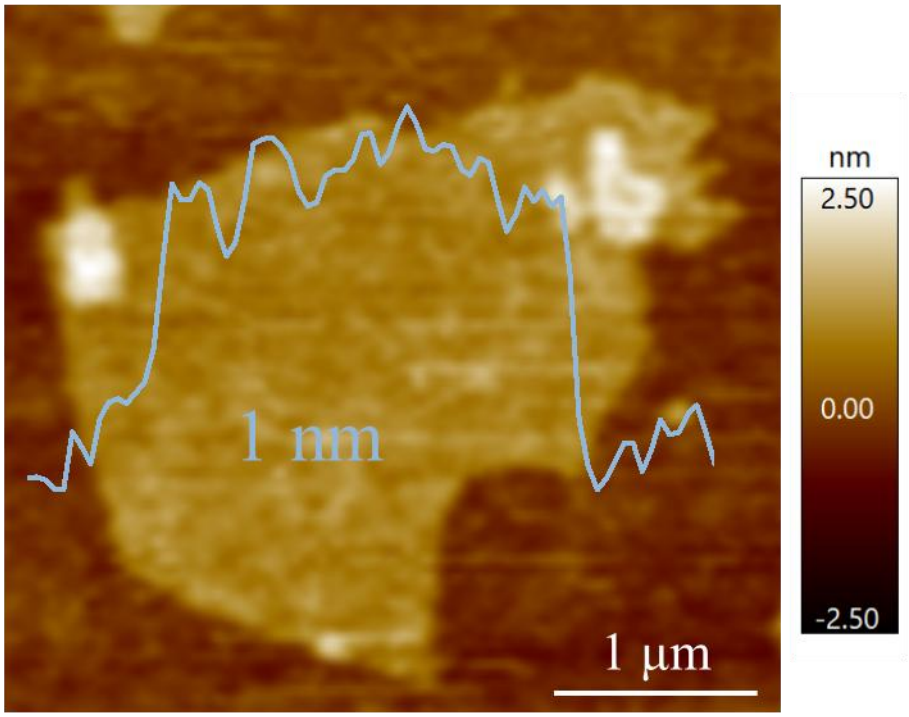

Supplementary Fig. 1. AFM image of GO nanosheet.

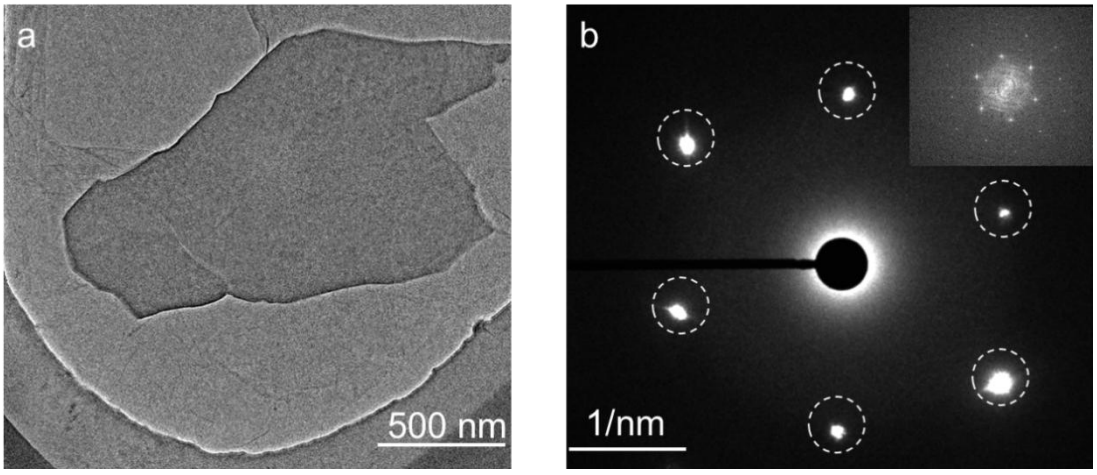

Supplementary Fig. 2. TEM image (a) and SEAD (b) of GO nanosheet.

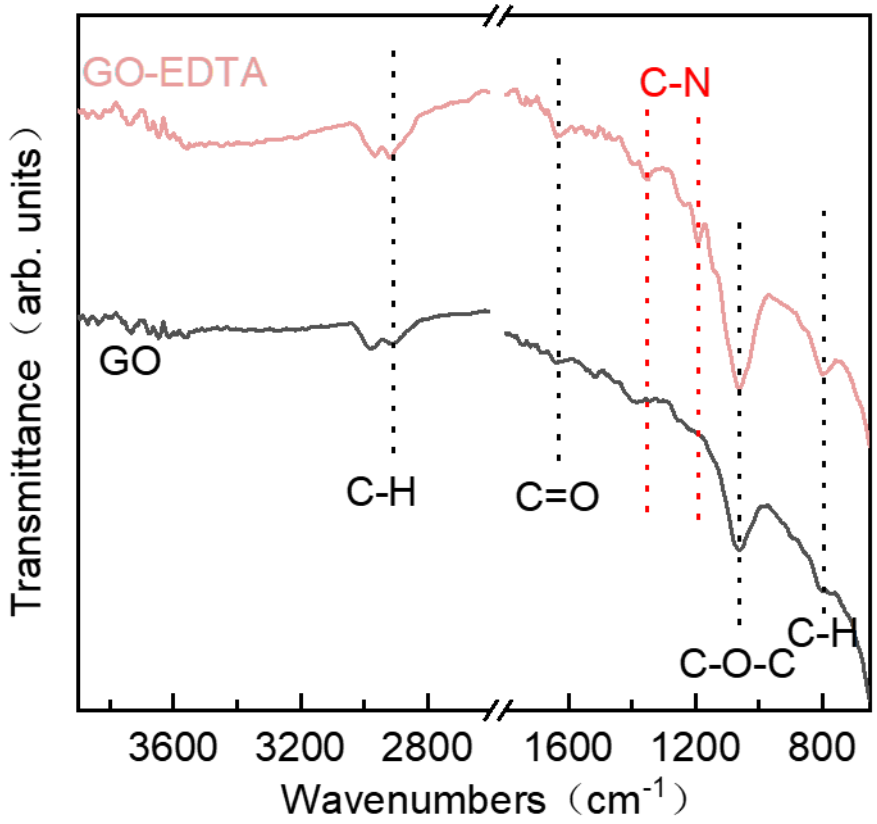

Supplementary Fig. 3. FTIR spectrum of the GO and GO-EDTA-1.5.

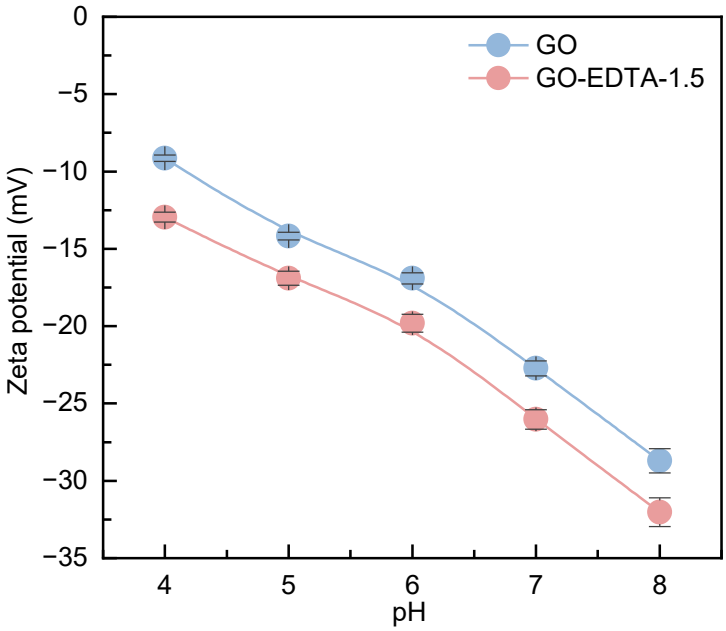

Supplementary Fig. 4. Zeta potential of the GO and GO-EDTA-1.5.

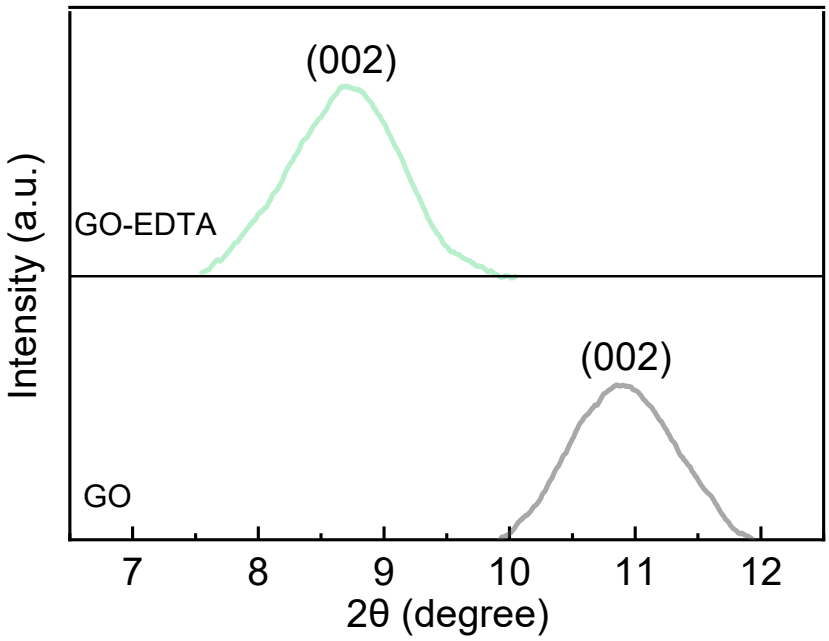

Supplementary Fig. 5. XRD patterns of the GO and GO-EDTA-2.0.

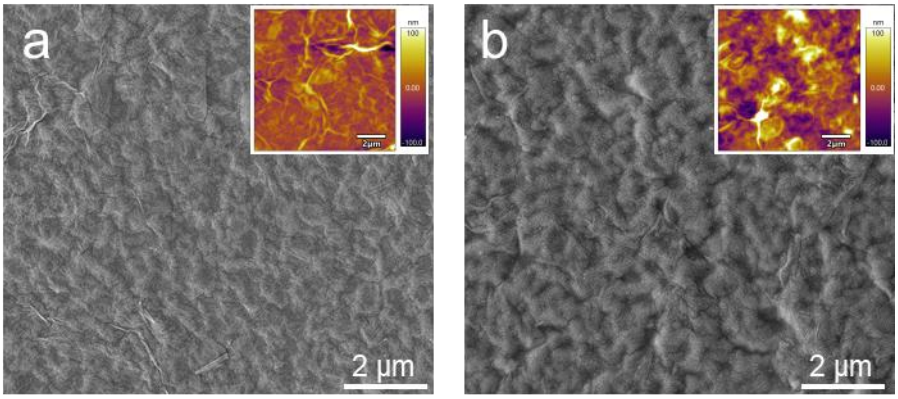

Supplementary Fig. 6. SEM images of (a) GO and (b) GO-EDTA-1.5, inset: corresponding AFM image.

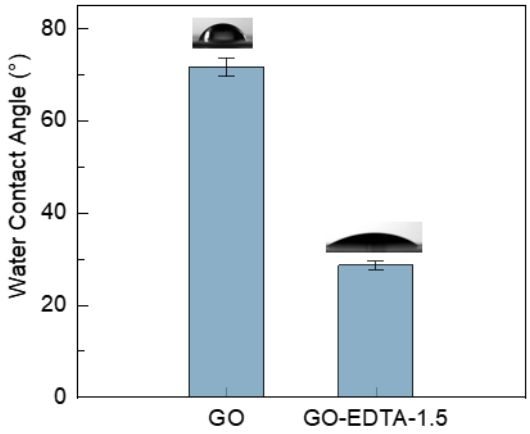

Supplementary Fig. 7. Water contact angle of GO and GO-EDTA-1.5.

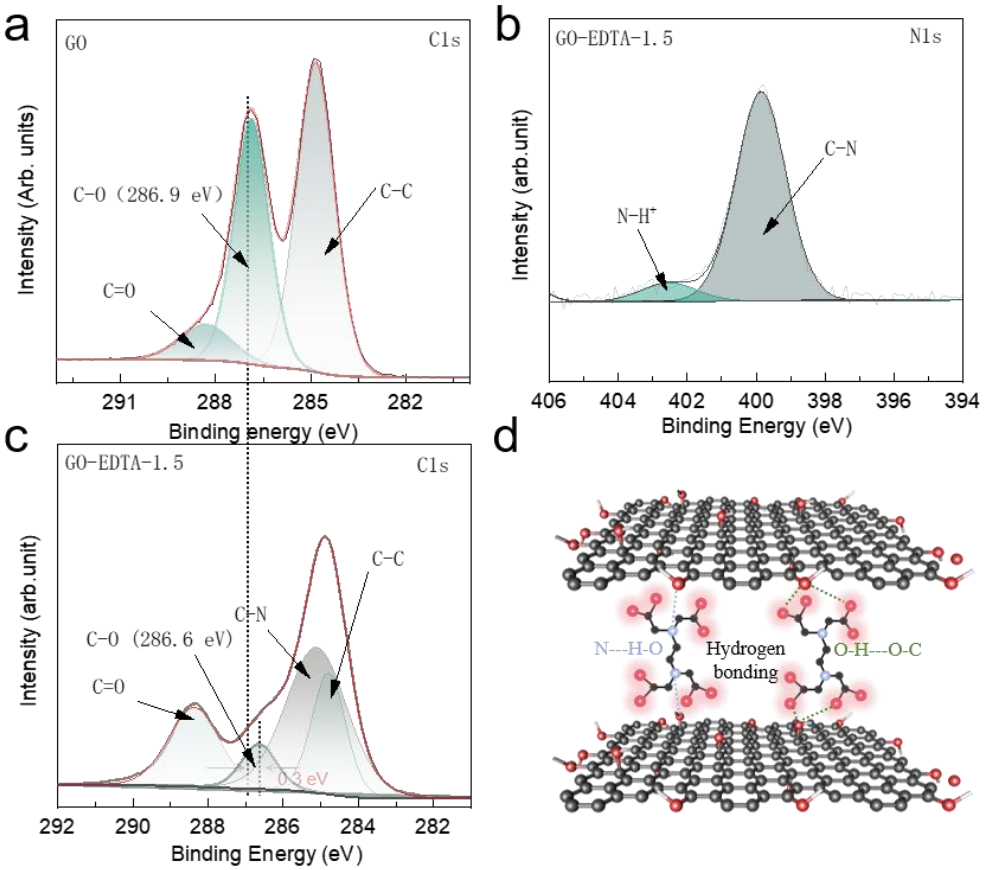

Supplementary Fig. 8. (a) C1s XPS spectra of GO, N1s(b) and C1s (c) XPS spectra of GO-EDTA-1.5, (d) Schematic diagram of the possible crosslinking mechanism between GO nanosheets and EDTA molecules.

The leftward shift of the C-O bond indicates a decrease in binding energy, suggesting the formation of hydrogen bonds between the C-O groups on GO nanosheet and the H groups on EDTA. The N-H present in N1s indicates that the N atom on EDTA forms hydrogen bonds with the H on GO nanosheet (Xu et al., 2024).

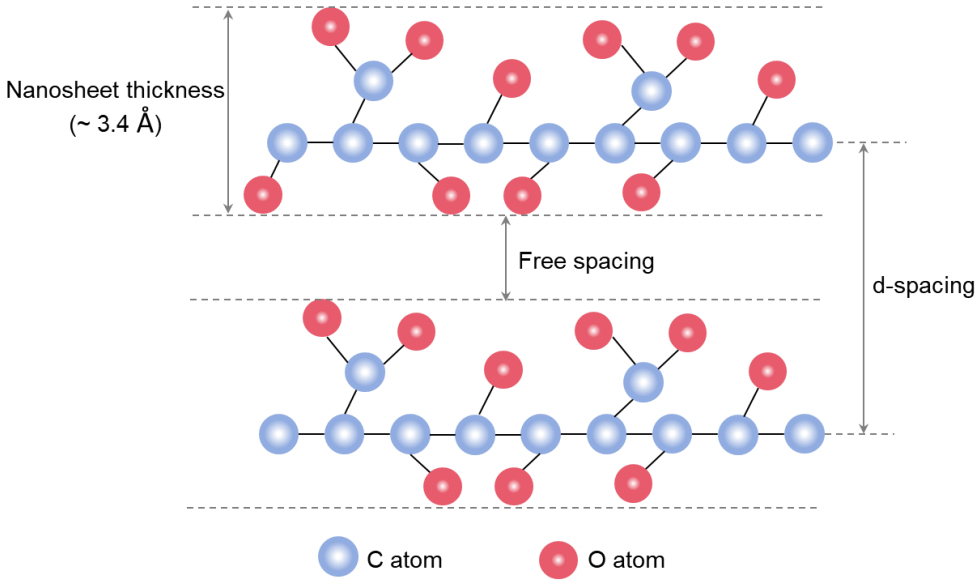

Supplementary Fig. 9. Schematic diagram of free spacing calculation.

The d-spacing calculated by XRD minus the thickness of the monolayer GO nanosheet of 3.4 Å is the free spacing (Chen et al., 2017).

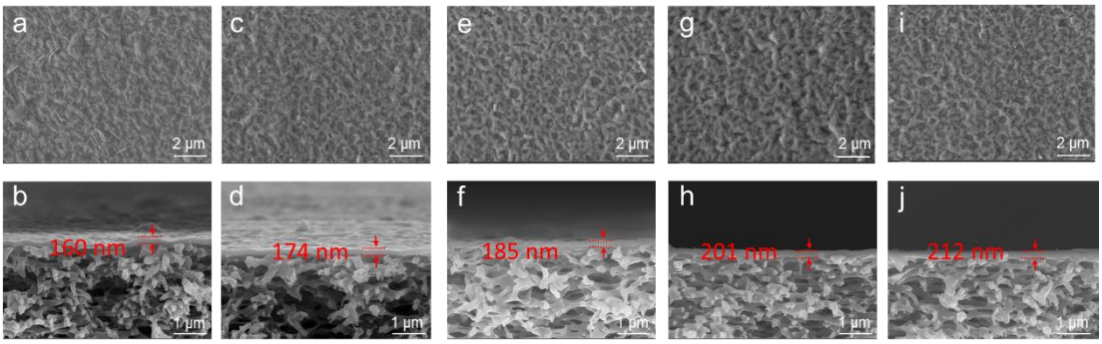

Supplementary Fig. 10. Surface and cross section SEM images for GO (a and b), GO-EDTA-0.5 (c and d), GO-EDTA-1.0 (e and f), GO-EDTA-1.5 (g and h) and GO-EDTA-2.0 (i and j) membranes.

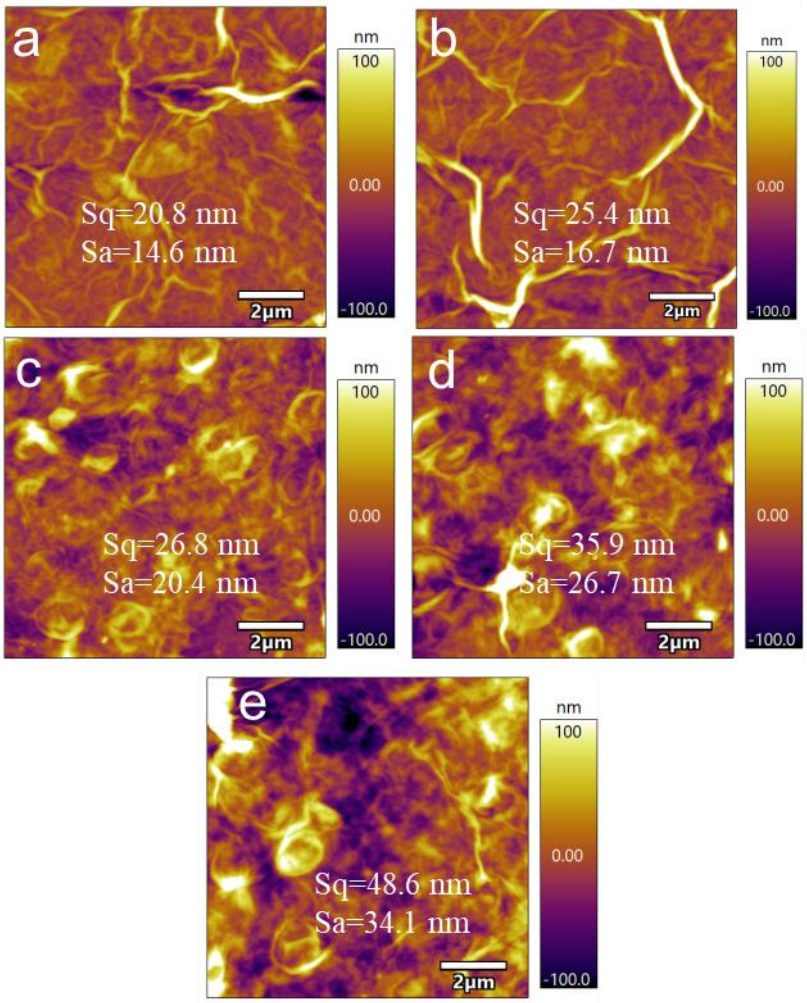

Supplementary Fig. 11. AFM images for GO(a), GO-EDTA-0.5 (b), GO-EDTA-1.0 (c), GO-EDTA-1.5 (d) and GO-EDTA-2.0 (e) membranes.

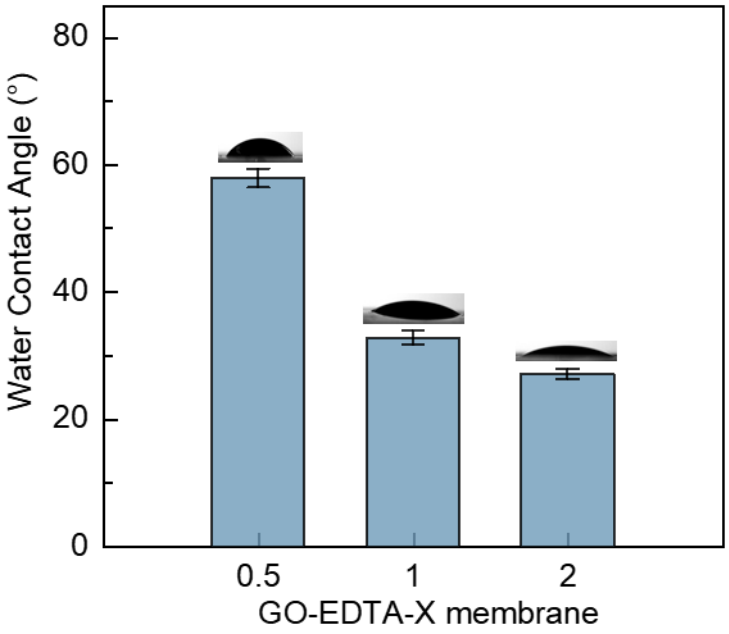

Supplementary Fig. 12. Water contact angle of GO-EDTA-0.5, GO-EDTA-1 and GO-EDTA-2.

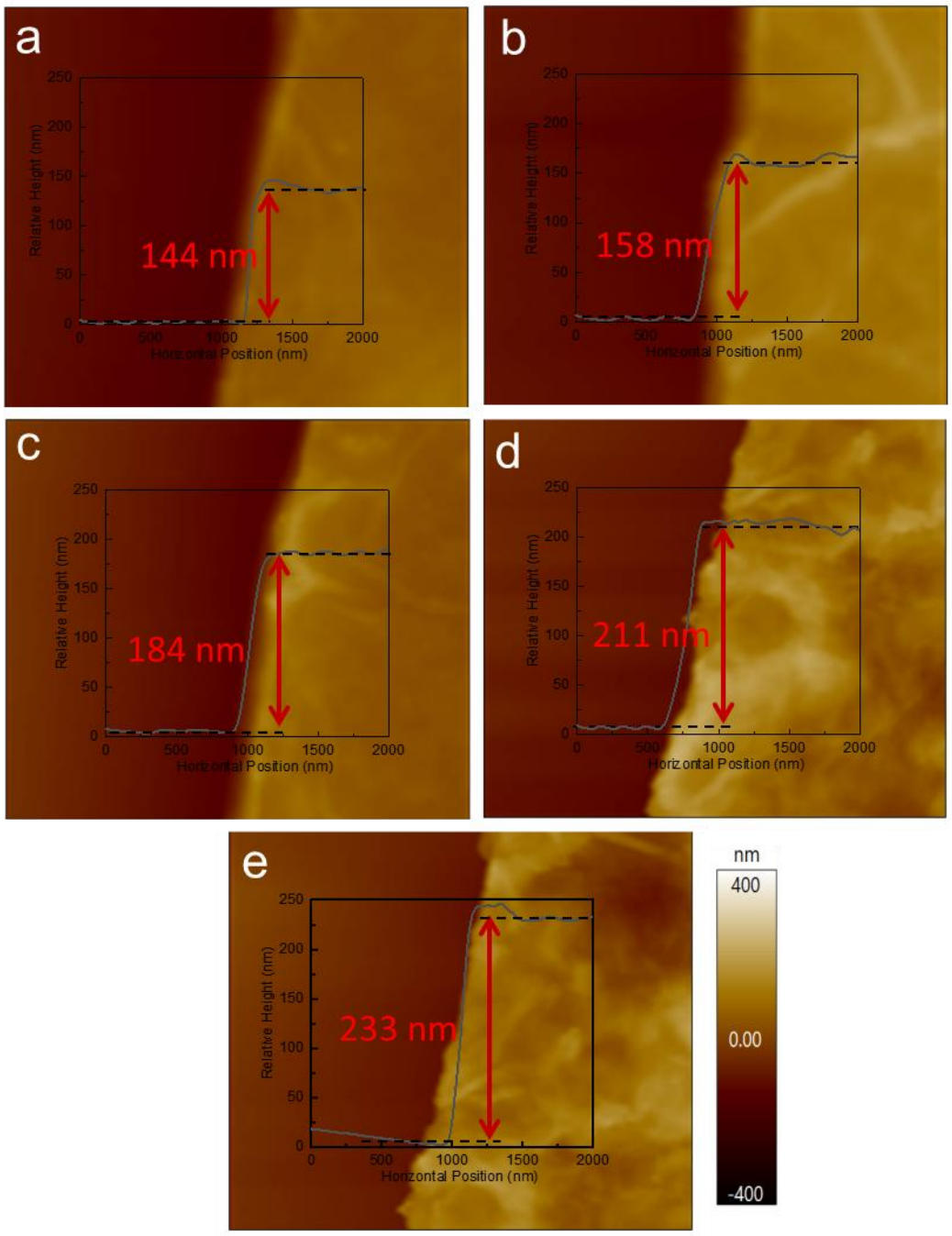

Supplementary Fig. 13. AFM images of cross section for GO(a), GO-EDTA-0.5 (b), GO-EDTA-1.0 (c), GO-EDTA-1.5 (d) and GO-EDTA-2.0 (e) membranes.

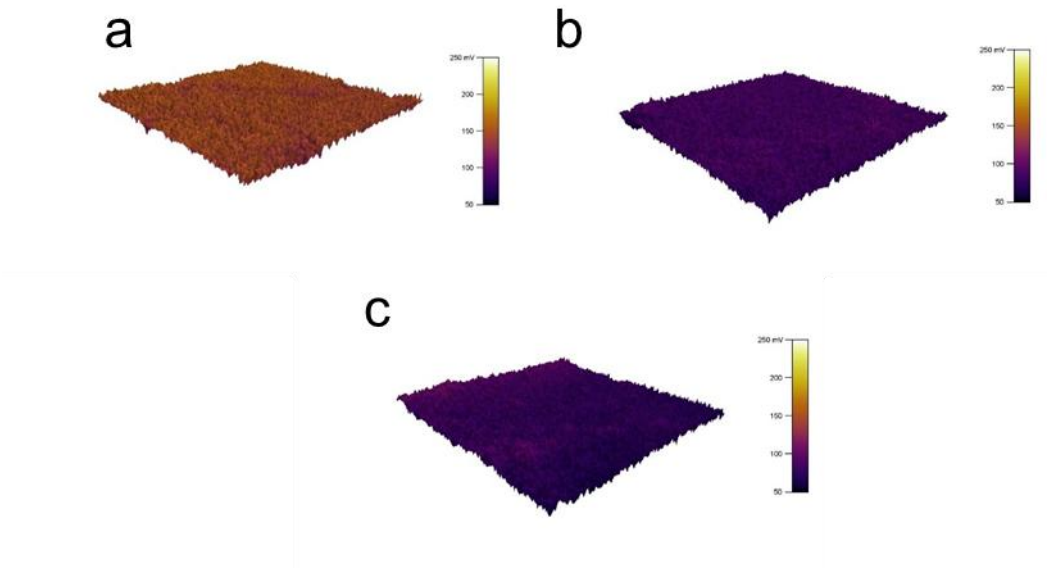

Supplementary Fig. 14. Surface potential for GO-EDTA-0.5(a), GO-EDTA-1.0 (b) and GO-EDTA-2.0 (c) membranes by KPFM.

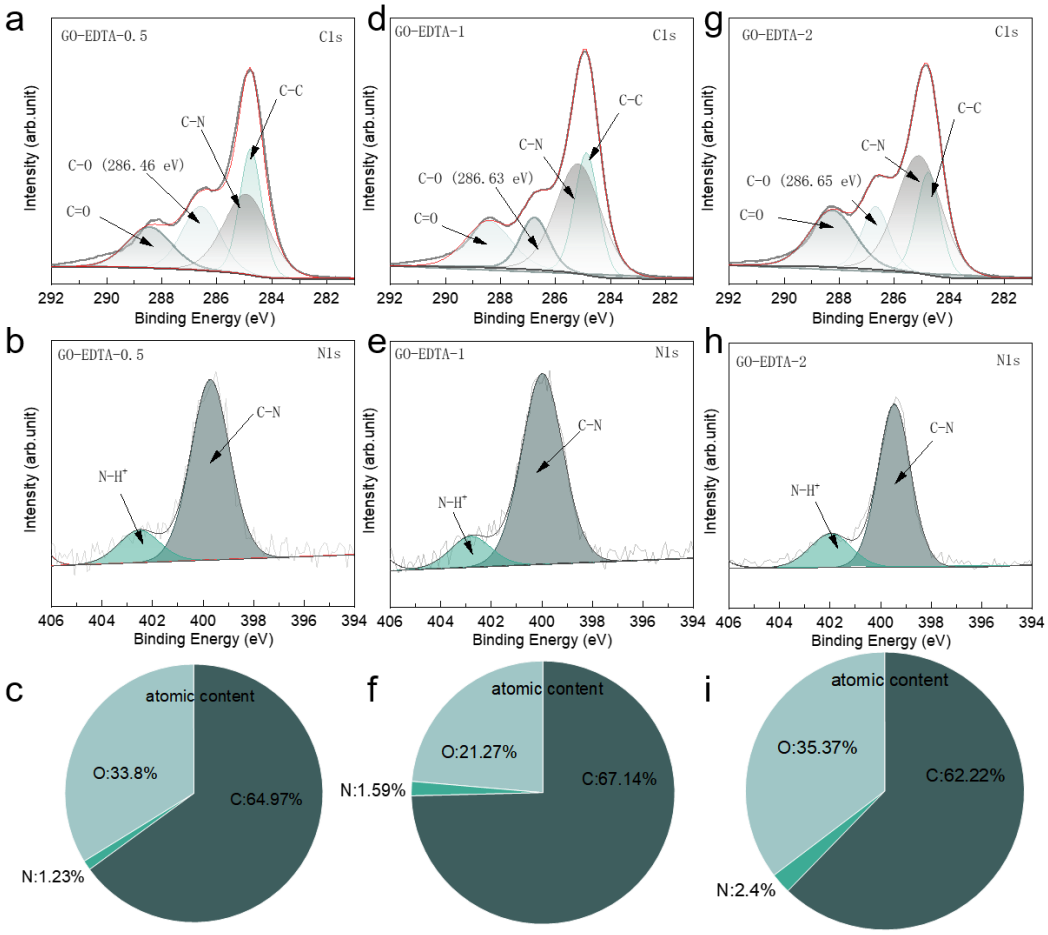

Supplementary Fig. 15. XPS spectrum of GO-EDTA-0.5, GO-EDTA-1 and GO-EDTA-2. C1s (a), N1s(b) and elemental ratio (c) of GO-EDTA-0.5. C1s (d), N1s(e) and elemental ratio (f) of GO-EDTA-1. C1s (g), N1s(h) and elemental ratio (i) of GO-EDTA-2.

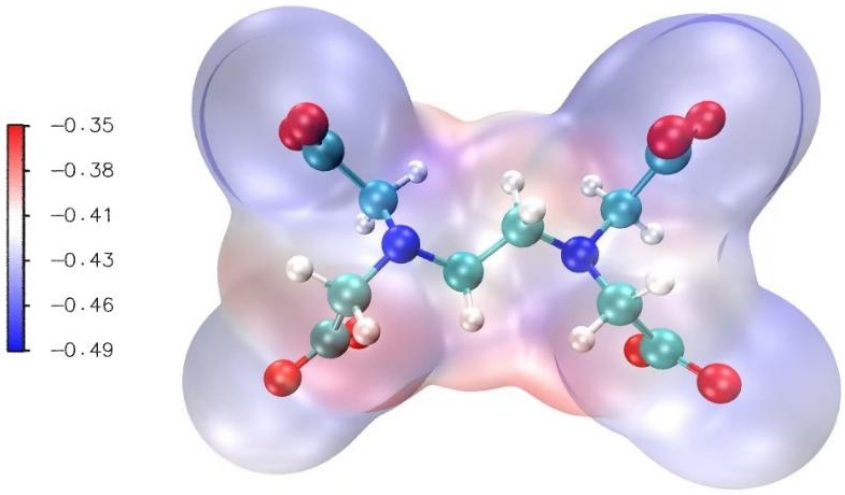

Supplementary Fig. 16. Electrostatic potential of EDTA molecular.

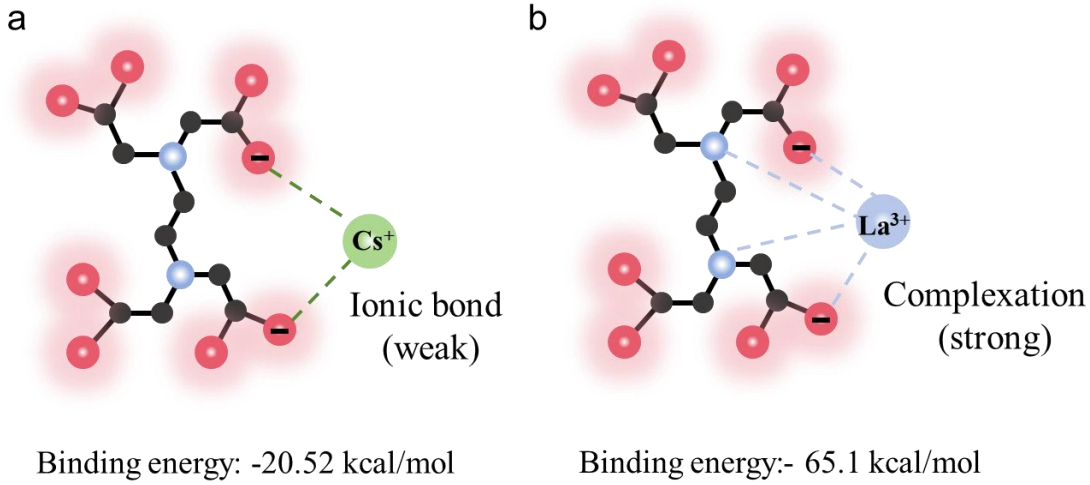

Supplementary Fig. 17. Binding energy between EDTA and Cs^+ (a), La^{3+} (b).

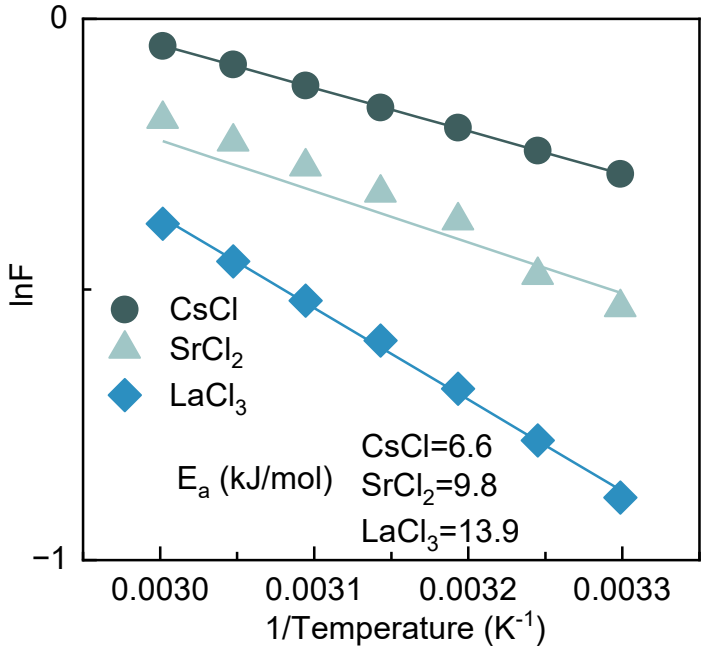

Supplementary Fig. 18. E_a of different ions for GO membrane.

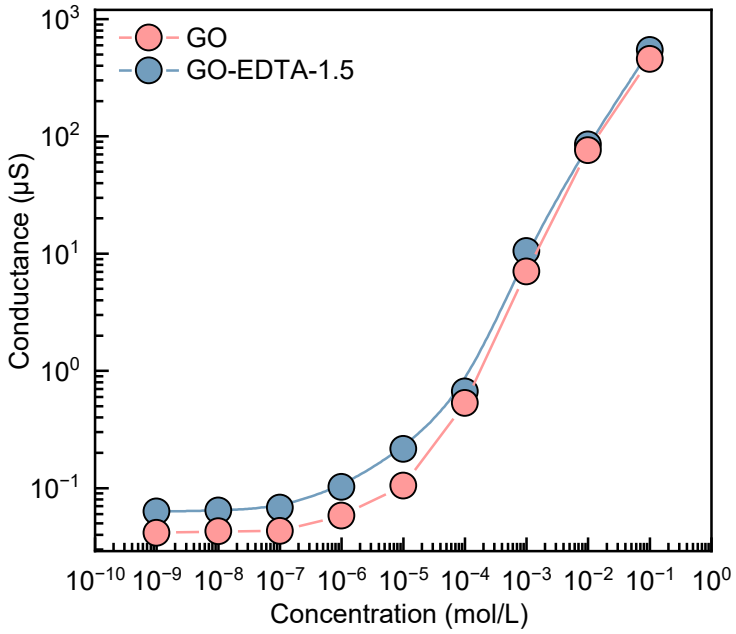

Supplementary Fig. 19. Conductance of CsCl of different concentration for GO and GO-EDTA-1.5 membrane.

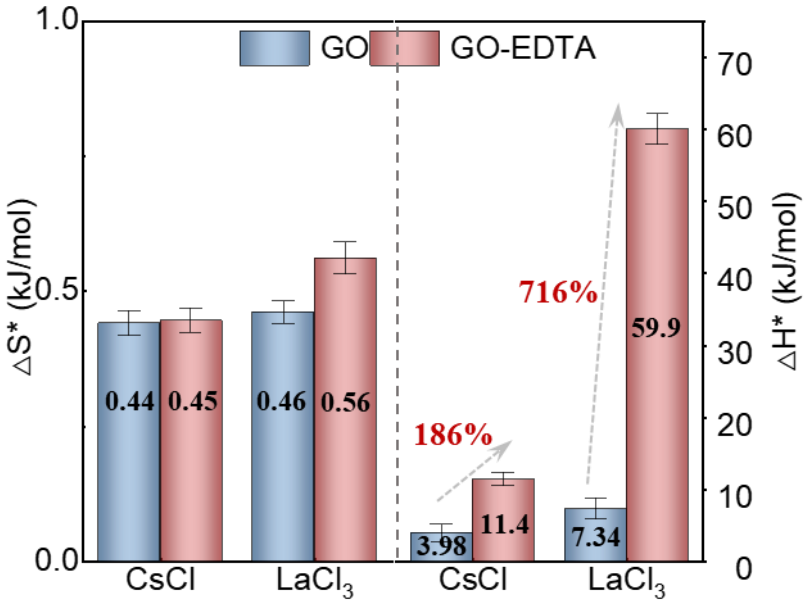

Supplementary Fig. 20. ΔS and ΔH of CsCl and $LaCl_3$ for GO and GO-EDTA.

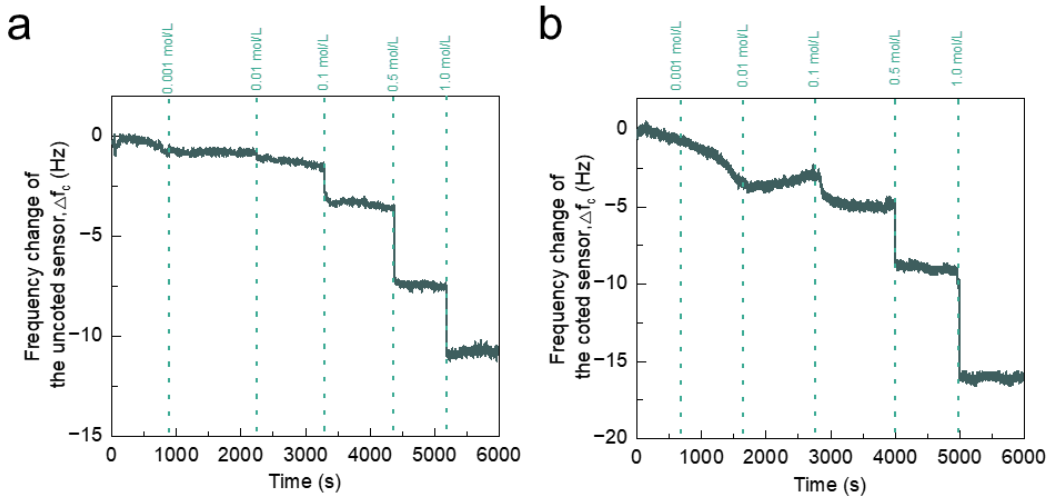

Supplementary Fig. 21. Representative QCM results. Frequency changes of sensors with different CsCl concentrations for (a) bare (control) sensor and (b) sensor coated with GO-EDTA-1.5 membrane. The frequency change was measured at 5 different CsCl concentrations (i.e., 0.001, 0.01, 0.1, 0.5, and 1.0 mol/L). At each concentration, once the frequency change was stabilized (~20 min), the salt concentration was increased. At last, DI water was applied to rinse the sensors and verify the baseline. In panel (b), the frequency change (Δfs) increases with solution concentration as more salts partition into the sensor. In panel (a), the frequency change (Δfc) also increases with solution concentration because solution properties (e.g., density and viscosity) vary with concentration. The real frequency change caused by salt partitioning (Δfs, p) is the difference between the frequency changes in panels (a) and (b) (i.e., Δfs, $p = \Delta fs - \Delta fc$). With the calculated Δfs, p, the mass of salt partitioning in the GO-EDTA membrane can be determined by the Sauerbery relationship (Zhou et al.).

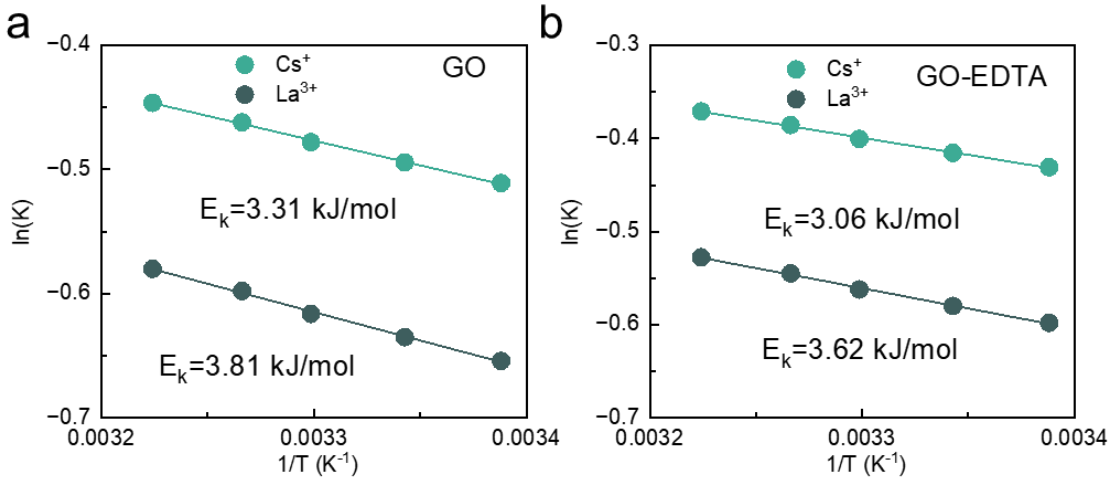

Supplementary Fig. 22. Partition energy barrier of GO (a) and GO-EDTA-1.5 (b) membranes.

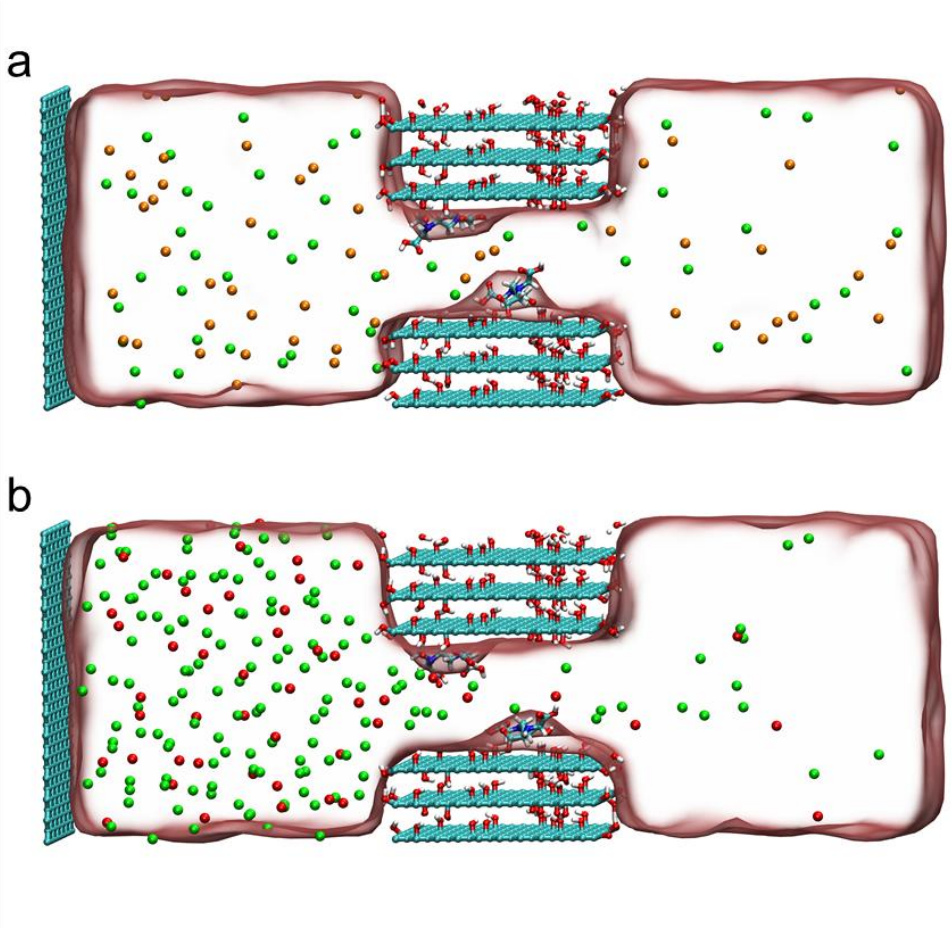

Supplementary Fig. 23. Molecular dynamics simulation model. Diffusion model of CsCl (a) and $LaCl_3$ (b) in the GO-EDTA channel.

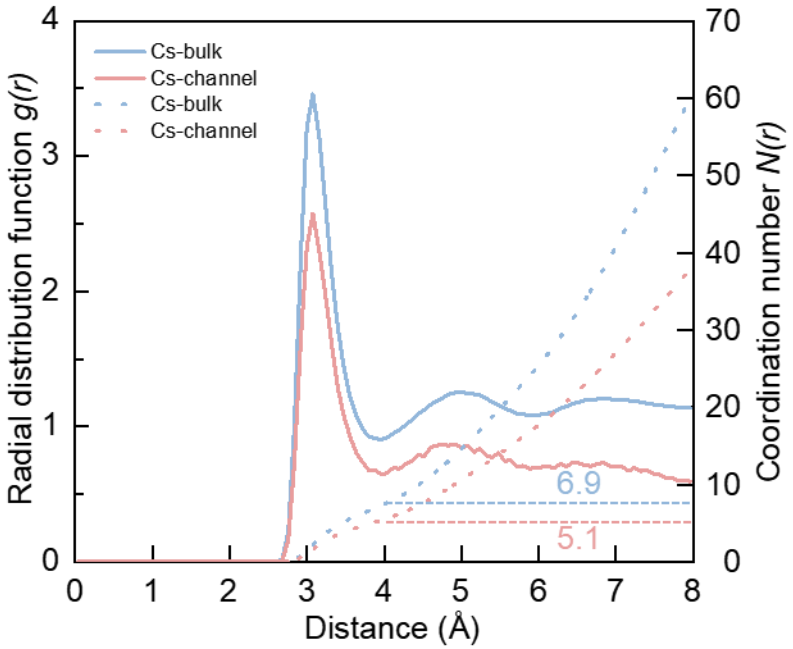

Supplementary Fig. 24. The radial distribution function and coordination number of Cs^+ in the bulk solution and GO-EDTA channels.

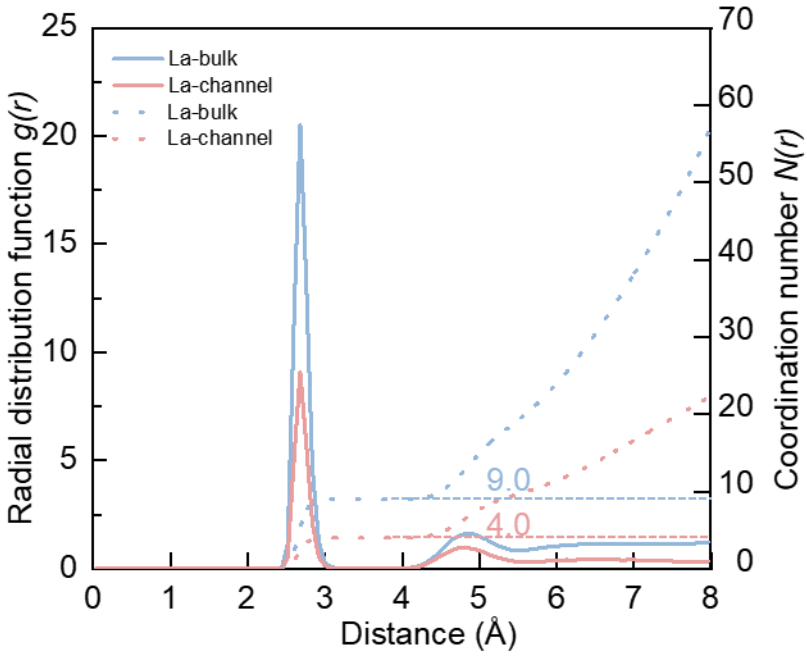

Supplementary Fig. 25. The radial distribution function and coordination number of La^{3+} in the bulk solution and GO-EDTA channels.

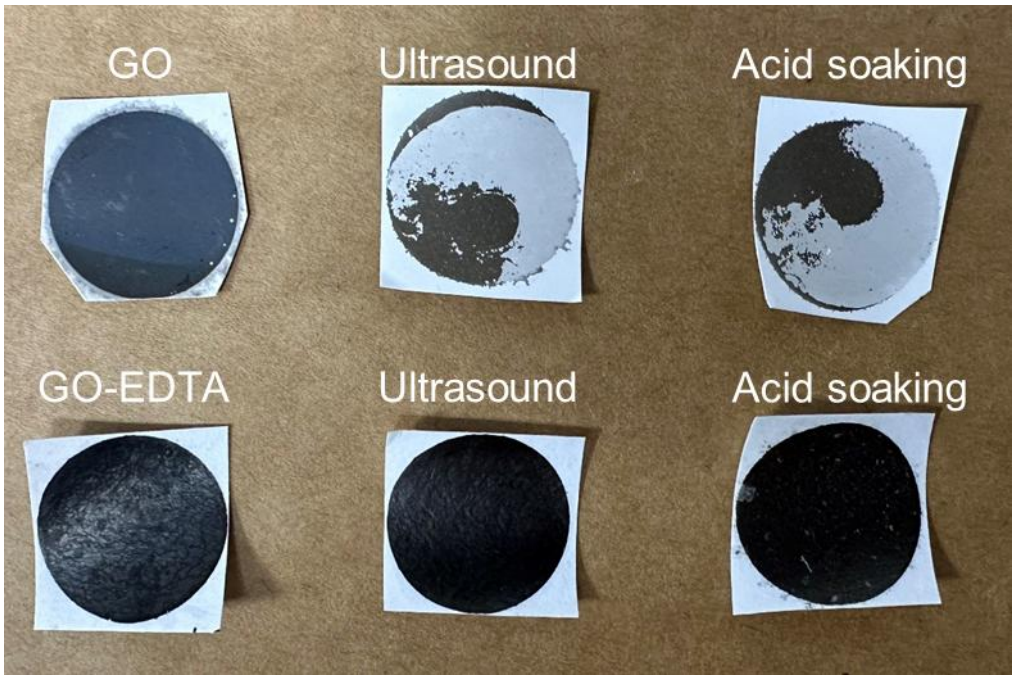

Supplementary Fig. 26. Photos of Original, ultrasonic treatment and acid soaking treatment for GO and GO-EDTA membrane.

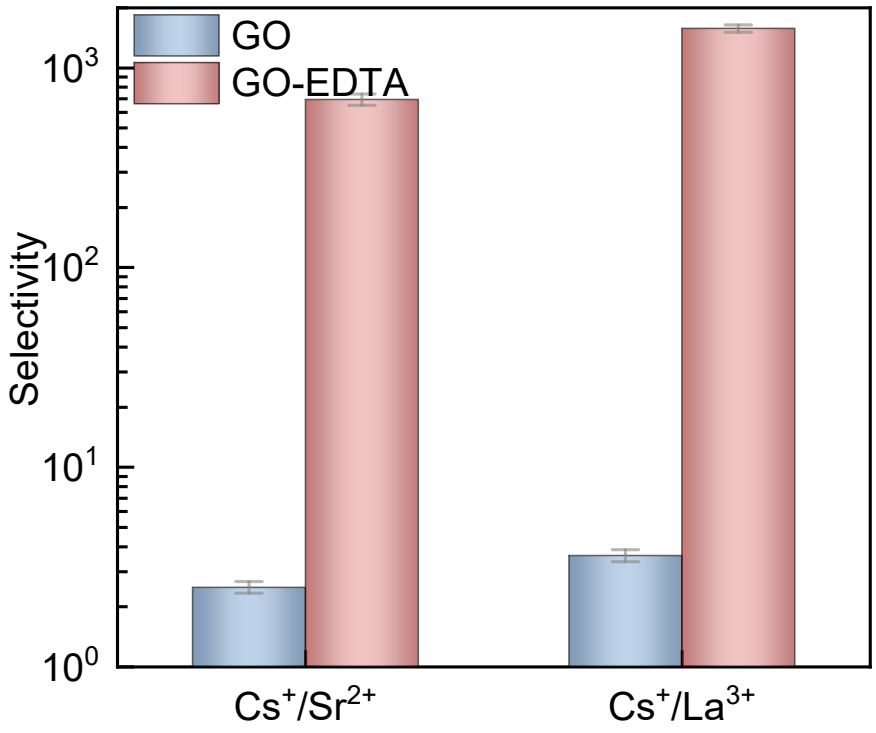

Supplementary Fig. 27. Ion selectivity of GO and GO-EDTA membranes in electrodialysis testing methods.

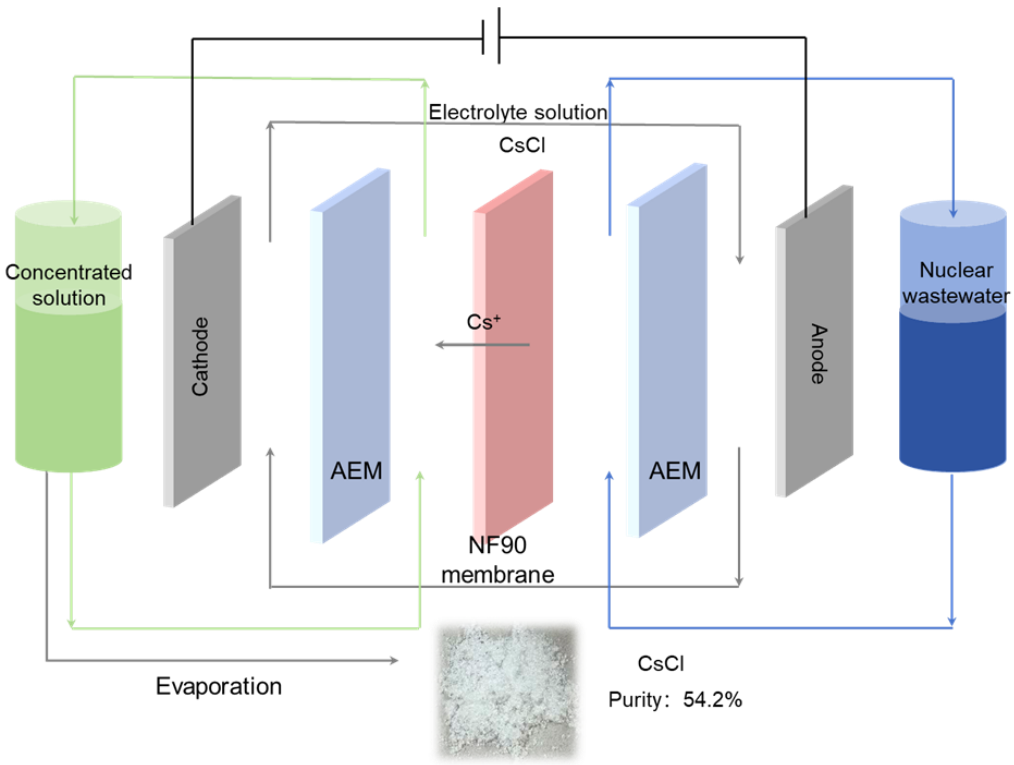

Supplementary Fig. 28. Schematic diagram of the application of commercial NF90 membrane in nuclear wastewater treatment and CsCl recovery.

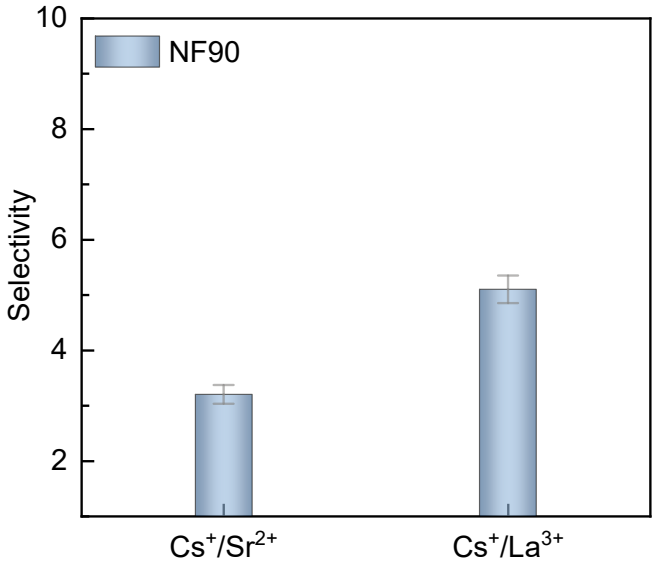

Supplementary Fig. 29. Ion-selective of commercial NF90 membrane in the treatment of nuclear wastewater by electrodialysis testing methods.

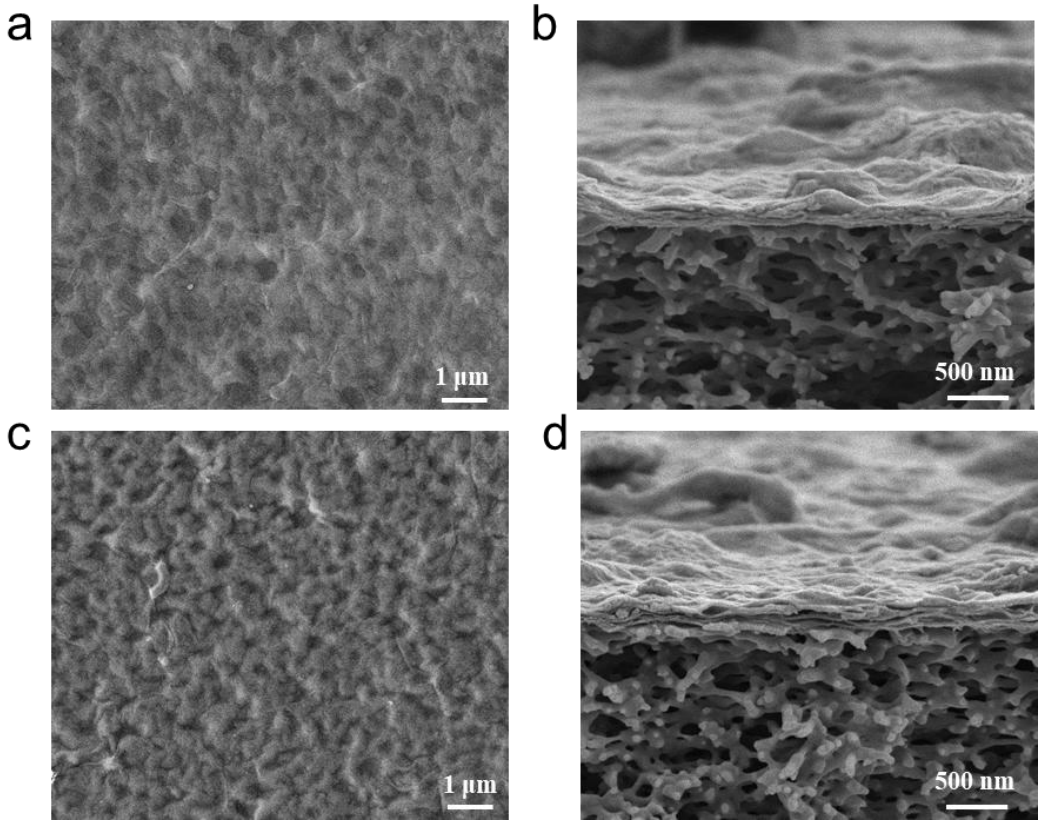

Supplementary Fig. 30. SEM images of the surface (a, c) and cross-section (b, d) of the GO-EDTA membrane after irradiation treatment. The radiation doses for a and b are 10 kGy, the radiation doses for c and d are 100 kGy.

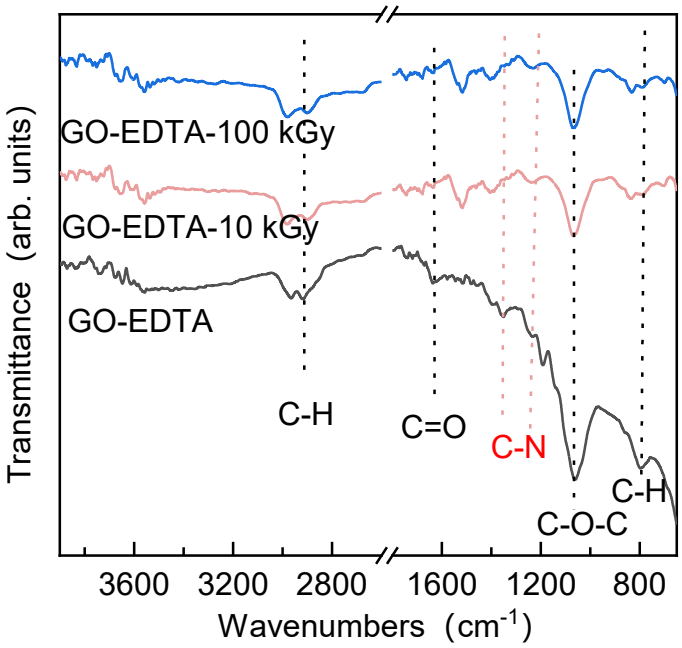

Supplementary Fig. 31. FTIR spectrum of the GO-EDTA and GO-EDTA membrane after irradiation treatment.

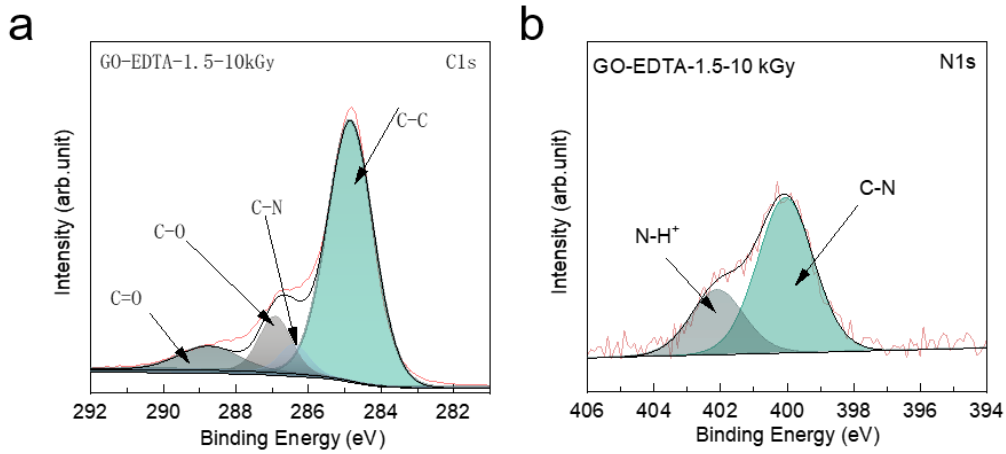

Supplementary Fig. 32. C1s (a) and N1s (b) spectrum of the GO-EDTA membrane after irradiation treatment.

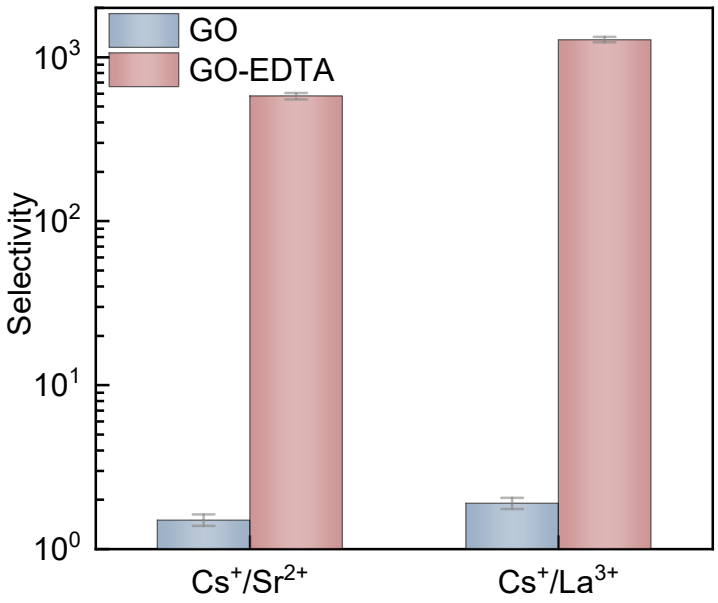

Supplementary Fig. 33. Ion selectivity of GO and GO-EDTA membranes after γ-ray irradiation treatment (100 kGy).

Supplementary Table 1. The physical properties of related ions in this study.

Ion species	Ionic radius[nm]	Hydrated ionic radius[nm]
H^+	0.115	0.28
K^+	0.133	0.331
Li^+	0.06	0.382
Na^+	0.08	0.358
Cl^-	0.181	0.332
Mg^{2+}	0.066	0.46
Al^{3+}	0.054	0.475
Cs^+	0.169	0.30
Sr^{2+}	0.126	0.41
La^{3+}	0.103	0.45

Supplementary Table 2. Comparison of the CsCl permeance and Cs^+/Sr^{2+} selectivity of several membranes reported in the literature.

Membrane	CsCl permeance （mol/(m^2 h)）	Cs^+/Sr^{2+} selectivity	reference
pGO	0.8	120	(Wang and Liang, 2024)
GO	0.3	20	(Wang and Liang, 2024)
PEI-UiO-66-NH_2/GO membranes	/	12	(Li et al., 2024)
HBAB-TAPA-COF	0.33	13.3	(Liu et al., 2024)
GO	/	3.3	(Ma et al., 2017)
GOM	0.069	3.27	(Fan et al., 2023)
OGRM	0.085	2.34	(Fan et al., 2023)
FJSMKCGTS	/	4.68	(Tang et al., 2024)
GO-EDTA (This work)	0.325	485	/

Supplementary References

Chen L, Shi G, Shen J, Peng B, Zhang B, Wang Y, Bian F, Wang J, Li D, Qian Z, Xu G, Liu G, Zeng J, Zhang L, Yang Y, Zhou G, Wu M, Jin W, Li J, Fang H (2017). Ion sieving in graphene oxide membranes via cationic control of interlayer spacing. Nature, 550(7676): 380-383

Fan Q, E Z, Shi L, Lu Z, Li P, Liang J (2023). Non-swelling oxidized graphene ribbon membrane for the effective separation of cesium and strontium from radioactive liquid waste. Journal of Membrane Science, 680: 121727

Li C, Li Z, Guan K, Chiao Y-H, Zhang P, Xu P, Gonzales R R, Hu M, Mai Z, Yoshioka T, Matsuyama H (2024). Polyethylenimine-assisted preparation of Zr-MOF/GO membranes for radionuclide separation. Desalination, 592: 118118

Liu Q, Liu M, Zhang Z, Yin C, Long J, Wei M, Wang Y (2024). Covalent organic framework membranes with vertically aligned nanorods for efficient separation of rare metal ions. Nature Communications, 15(1): 9221

Ma F, Li Z, Zhao H, Geng Y, Zhou W, Li Q, Zhang L (2017). Potential application of graphene oxide membranes for removal of Cs(I) and Sr(II) from high level-liquid waste. Separation and Purification Technology, 188: 523-529

Tang J-H, Jia S-Q, Liu J-T, Yang L, Sun H-Y, Feng M-L, Huang X-Y (2024). “Ion-imprinting” strategy towards metal sulfide scavenger enables the highly selective capture of radiocesium. Nature Communications, 15(1): 4281

Wang S, Liang S (2024). Acid response nanochannels of graphene oxide membranes for fast nuclide ions separation. Separation and Purification Technology, 328: 125086

Xu R, Zhang J, Kang Y, Yu H, Zhang W, Hua M, Pan B, Zhang X (2024). Reversible pH-Gated MXene Membranes with Ultrahigh Mono-/Divalent-Ion Selectivity. Environmental Science & Technology, 58(15): 6835-6842

Zhou X, Wang Z, Epsztein R, Zhan C, Li W, Fortner J D, Pham T A, Kim J-H, Elimelech M Intrapore energy barriers govern ion transport and selectivity of desalination membranes. Science Advances, 6(48): eabd9045